C.P. No. 1077

C.P. No. 1077

MINISTRY OF TECHNOLOGY

AERONAUTICAL RESEARCH COUNCIL

CURRENT PAPERS

The Calculation of Three-Dimensional Turbulent Boundary Layers Part IV: Comparison of Measurements with Calculations on the Rear of a Swept Wing

by

N.A. Cumpsty and M.R. Head

Cambridge University Engineering Department

LONDON: HER MAJESTY'S STATIONERY OFFICE

1970

PRICE 9s 0d [45p] NET

C.P. No.1077*

March, 1969

The calculation of three-dimensional turbulent boundary layers. Part IV: Comparison of measurements with calculations on the rear of a swept wing

by N.A. Cumpsty† and M.R. Head

Cambridge University Engineering Department

Summary

A boundary layer development was measured on the rear of a wing swept at 61°. The measurements approximately followed an external streamline from the minimum pressure to the neighbourhood of the separation line. Unfortunately the flow was found to be surprisingly sensitive to traverse gear interference. Moreover, the constraint imposed by the wind tunnel walls was sufficient to throw grave doubts on the use of the assumption of constant spanwise velocity to compute the external flow behaviour from the measured pressure distribution.

Comparison of the measurements with calculations using the method proposed by Cumpsty and Head[1] showed the growth of streamwise momentum thickness, form parameter and crossflow to be seriously underestimated. However, only a small adjustment to the spanwise velocity outside the boundary layer over the rear of the wing was sufficient to bring the results into tolerable agreement. The necessity for such an adjustment to the spanwise velocity may be plausibly explained by the effect of tunnel constraints.

---

*Replaces A.R.C.31 029

†Now at Rolls-Royce Ltd., Hucknall, Nottingham.

Notation

x	distance measured around the surface from the minimum pressure in a direction normal to the generators of the wing
ζ	distance measured normal to the surface
X	distance measured normal to leading edge in plane of chord
Z	distance of point on wing surface from chord plane, measured normal to chord plane
U_∞	undisturbed velocity
U_s	resultant velocity outside the boundary layer
$U_{1\infty}$	velocity outside the boundary layer in the x-direction
V	velocity outside the boundary layer in the spanwise direction
V_{le}	velocity outside the boundary layer along the leading edge
u	time-mean streamwise velocity within the boundary layer
v	time-mean crossflow velocity
δ_1^*	$\int_o^\infty (1 - u/U_s)d\zeta$ streamwise displacement thickness
θ_{11}	$\int_o^\infty (1 - u/U_s)u/U_s d\zeta$ streamwise momentum thickness
δ_2^*	$\int_o^\infty - v/U_s d\zeta$
θ_{12}	$\int_o^\infty (1 - u/U_s)v/U_s d\zeta$
θ_{21}	$\int_o^\infty - uv/U_s^2 d\zeta$
θ_{22}	$\int_o^\infty - v^2/U_s^2 d\zeta$
H	δ_1^*/θ_{11}, streamwise form parameter
β	angle between the projection onto the surface of the flow direction outside the boundary layer and the limiting time-mean direction as surface is approached
$R_{\theta 11}$	$U_s\theta_{11}/\nu$
τ_w	wall shear stress in streamwise direction
u	$(\tau_w/\rho)^{\frac{1}{2}}$, streamwise friction velocity

ρ	air density
ν	air kinematic viscosity
p	static pressure
c	wing chord (measured normal to leading edge)

1. Introduction

One of the most pressing requirements of boundary layer theory is that it should be able to predict the development of turbulent boundary layers on swept wings. For wings of large aspect ratio it seems reasonable to ignore the effect of spanwise variations and treat the wing as though it were infinite. In this case the difficulties in calculating the development are greatly reduced.

Such calculations have been performed by Cumpsty and Head[1], by Smith[2] and more recently by Thompson[3] as well as several other workers. These calculations all rely heavily on the use of two-dimensional concepts to represent the streamwise boundary layer. In particular, the two-dimensional calculation method proposed by Head[4] has been found to be readily generalised; in this approach the rate of entrainment of irrotational fluid into the boundary layer is assumed to depend on a form parameter of the streamwise velocity profile.

The calculations by Cumpsty and Head were performed for a hypothetical wing since existing measurements were felt to be inadequate for a useful comparison to be made. Smith, on the other hand, compared his calculations with measured boundary layer developments on a flat plate on which a pressure gradient was imposed by a circular cylinder fitted with a Thwaites flap, both plate and cylinder being swept at 26.5°. On the whole the measure of agreement obtained was rather unsatisfactory and it was apparent that,without further evidence, such calculations could not be accepted as giving even a reasonable approximation to the true development of three-dimensional turbulent boundary layers. A particularly disturbing feature was the inaccurate prediction of the development of the streamwise momentum thickness,

θ_{11}, which two-dimensional experience would suggest should be predicted with at least moderate accuracy.

Although the present authors had recognised the need for definitive boundary layer measurements on swept wings, the negative implications of Smith's results provided an additional incentive. A wing swept at 60° had already been made for the measurements of leading edge flow (Cumpsty and Head[5]), and when the wing was designed the possibility of measurements on the rear was foreseen. However, had the wing been designed solely for measurements over the rear, a lower thickness-chord ratio and a more moderate angle of sweep would have been chosen. Although the aspect ratio was large, it still appears that the tunnel roof and floor (between which the wing was mounted) produced substantial constraints. Moreover the flow was affected by the presence of the traverse gear even after this was modified to present a very small obstruction to the flow.

At the outset these measurements had been intended to provide a definitive set of results for comparison with calculations. In the event, however, too many uncertainties arose for this to be reasonably claimed, but it has been thought worthwhile to present the measurements for two reasons; first, because they represent one of the very few sets of measurements made along an external streamline on a swept wing from the minimum pressure to close to the separation line , and, second, because they demonstrate some of the major experimental difficulties encountered in making accurate three-dimensional measurements. Moderately good agreement with the calculations has been found, but only after some allowance has been made in the calculations for the possible

effect of wind tunnel constraints.

2. The wing and traverse gear

Because the wing had originally been designed for measurements of the attachment-line boundary layer, the leading-edge radius and angle of sweep were both large. The wing was constructed of a 228 mm diameter brass pipe with a built-up fairing on the rear. This fairing was designed to blend with the pipe just forward of the point of maximum thickness with continuous slope and curvature. The ordinates of the surface along a line normal to the leading edge are given in Table 1.

The length of the wing along the leading edge was 2.44 m so that with a nominal sweep of 60° it fitted between the roof and floor of the tunnel working section, which were 1.22 m apart. The working section was 1.68 m wide and about 3.0 m long. A sketch of the wing in the tunnel is shown in Figure 1. Two sets of pressure tappings were set in the wing in rows normal to the leading edge. Over the front of the wing they were spaced 10° apart, as measured from the centre of the pipe, whilst over the rear they were at approximately 25.4 mm intervals measured around the surface.

The traverse gear underwent considerable alteration during the course of the measurements. For the first set of measurements the operating mechanisms for displacing and rotating-in-yaw the hot wire were inside the working section and operated by Bowden cables, whereas for the later measurements the operating mechanisms were outside the tunnel. Figure 2 shows photographs of the unmodified original traverse gear and the slender traverse gear in position in the tunnel. The slender traverse gear used for the later measurements is probably the most aerodynamically

compact configuration possible with this type of measurement. Passing down the inside of the streamline strut there was, in addition to a 4.8 mm rod moving the hot wire, the coaxial cable leading to the hot wire. In each case the movement normal to the surface was obtained by rotating a micrometer head via a worm wheel and Bowden cable, and the angular motion was obtained by a worm wheel and gear train operated by a second Bowden cable. Distances could be measured to 0.025 mm and angles to 0.01°. It was impossible to eliminate backlash entirely in either mechanism and to minimise its effect settings were always made approaching from the same direction.

The traverse gear and hot wire were located relative to the wing surface by means of a bridge, clearly visible in Figure 2, with the whole traverse gear spring loaded against the surface. The axis of rotation passed midway between the legs of the bridge and the hot wire was located on the axis by means of a cranked stem. It was necessary to mount the traverse gear with its axis normal to the surface and the legs of the bridge were made adjustable in length to enable this to be done. The hot wire, a miniature Disa type, was about 1 mm long. It was carefully set parallel to the surface and, so that it could be brought in contact with the surface, the probe was inclined at about 12° to the surface.

The hot wire anemometer and linearizer were manufactured by Disa. The mean output voltage was recorded on a digital voltmeter, and it was found that the fluctuation in the output voltage was sufficiently reduced by a very simple resistance-capacitance circuit with a 2 second time constant.

3. Experimental details

3.1 General

The micrometer reading corresponding to the position of the surface was found by coating the surface in the traverse position with graphite from a soft pencil. Using a cathode ray oscilloscope as a very high resistance voltmeter and a $1\frac{1}{2}$ volt cell, a circuit was completed when the hot wire touched the surface. (The hot wire showed no apparent ill effects from this treatment.) In fact, with the tunnel running the probe vibrated and an intermittent contact was indicated over a range of about 0.05 mm. The limits of this range were highly repeatable and the effective position of the surface was taken as the mean of these readings.

The constant-temperature hot wire requires the largest current when the wire is normal to the flow direction, i.e. when the probe is aligned with the flow. The peak is rather flat-topped, however, and this approach does not give an accurate indication of the flow direction. The method used by Francis and Pierce[6] to measure flow direction was therefore adopted. The hot wire is yawed through an appreciable angle (30° was adopted here) from the approximate direction of the flow as determined from the position of maximum current. The time-mean output is recorded and the wire is then yawed in the opposite direction until the same output is obtained. Provided the hot wire is symmetrical the flow direction bisects the two yawed directions; if it is in any way asymmetric an error occurs. If this error can be assumed constant, it will not have any effect where (as here) the same method is used to obtain the direction of the flow outside the boundary layer. The direction measurements were repeatable to within 0.1°, but it became apparent that the yawing of the probe introduces an unknown interference effect. Furthermore the wire

must be parallel to the surface; any errors in this can lead to quite large errors in the measured direction close to the surface.

3.2 Compensation for changes in air temperature

It was found that the hot wire output was greatly affected by changes in air temperature produced by the work of the wind tunnel fan. To make satisfactory measurements it was necessary to run the tunnel for between 1 and 2 hours to allow the temperature of the air in the circuit to reach a comparatively steady value. In addition the tunnel was stopped briefly about half way through a traverse and the linearisor re-set. In this way the total drift from beginning to end of a traverse was kept down to the equivalent of about 1% of the free-stream velocity.

4. The experimental results

4.1 The overall flow

Preliminary measurements showed that the boundary layer separated some 200 mm from the trailing edge, measured along the surface. To give a rather greater extent of boundary layer development the wing was set at a negative incidence of about 1° and separation was delayed on the working side of the aerofoil to within 90 mm of the trailing edge for an appreciable part of the span. This angle of incidence has been used for all the measurements described here.

Figure 3 shows the pressure distributions measured at two spanwise positions. Away from the pressure minimum and separation line the agreement is very good. Oil flow confirmed that the separation line moved from the trailing edge at the upstream tappings to about 90 mm from the trailing edge for a considerable distance on either side of the downstream tappings. Two velocity

profiles measured at different spanwise positions (one 152 mm upstream, the other 254 mm downstream along the span from the pressure tappings) but the same distance from the trailing edge are compared in Figure 4. The profiles were measured with the original traverse gear, but this does not invalidate the conclusion that spanwise variation is locally very small.

For all the measurements described here the Reynolds number per metre, U_∞/ν, was 3.02×10^6.

4.2 Boundary layer traverses with the original traverse gear

Using the traverse gear with the operating mechanism inside the working section, boundary layer traverses were made at seven positions approximately along an external streamline intersecting the downstream pressure tappings at mid-chord. For convenience, the positions of the boundary layer traverses are denoted by values of x, the distance in mm from the start of the adverse pressure gradient, measured around the surface of the wing in a direction normal to the leading edge. The trailing edge corresponds to $x = 396$ mm and the separation line to $x \doteq 304$ mm.

The overall properties of the profiles measured with this traverse gear are shown in Figures 5 and 6, together with results obtained using the modified traverse gears and the results of calculations. The displacement and momentum thicknesses show generally smooth variations but β (the angle between the flow direction at the boundary layer edge and the limiting flow direction as the surface is approached) is somewhat erratic. This almost certainly reflects the difficulty of measuring β.

4.3 Traverse gear interference

Although it had been suspected that the traverse gear might be influencing the flow, this was not apparent from the boundary

layer measurements or pressure distributions. As a check, however, a three-hole yaw probe was attached to the wing surface; by comparing the pressures in the three tubes with the traverse gear in place (with the axis directly above the mouths of the yaw probe), and removed, an estimate of the interference could be obtained. The yaw probe is strictly only accurate in unsheared flow, but a preliminary check had shown the calibration for direction was sensibly unchanged when the probe was attached to the surface under a turbulent boundary layer.

It came as something of a surprise to find that at $x = 248$ mm (close to where a traverse had been made) the flow direction changed by $8\frac{1}{4}°$ and the magnitude by 23% when the traverse gear was removed. Indeed, this was with the hot wire about 25 mm from the surface, and the probe aligned with the flow, i.e. in the attitude likely to give least interference. Paradoxically the changes were such that the flow was more nearly spanwise and the magnitude lower when the traverse gear was removed; the presence of the traverse gear delayed separation. A similar check at the pressure minimum showed changes of only $\frac{1}{2}°$ in flow direction and $1\frac{1}{2}\%$ in magnitude and it was therefore inferred that the large changes were associated with movement of the separation line.

A number of expedients were tried to reduce the interference. The original bridge was replaced by a much broader one and cylindrical parts of the traverse gear were faired. Finally the strut between the floor and ceiling, used to brace the traverse gear against the wing, was replaced by a strut against the tunnel wall. With this configuration at $x = 248$ mm the interference was reduced to 4° and 7% in direction and magnitude respectively. A boundary layer profile was measured with this configuration, but

it had become apparent that little further improvement would be possible without more radical changes.

It was at this time that the slender traverse gear was developed so that the operating mechanisms were entirely outside the tunnel. Again at $x = 248$ mm, with the hot wire 25 mm from the surface and the probe aligned with the flow, the direction and magnitude changed by 2° and 6% when the traverse gear was removed. With the traverse gear in the same position, but with the hot wire just above the yaw probe, the direction changed by $3\frac{1}{2}$° and the magnitude hardly at all. The corresponding direction changes with the hot wire close to the surface but with the probe rotated 30° towards, and 30° away from, the spanwise direction were 5° and $1\frac{1}{2}$° respectively. Although these results cannot be considered wholly satisfactory they do represent a very marked improvement over those obtained with the original traverse gear. Indeed it seems probable that, when using this method of measurement near to three-dimensional separation lines, it will be impossible to make the interference effects completely negligible.

4.4 Boundary layer measurements with the slender traverse gear

The overall properties of the five profiles measured with the slender traverse gear are shown in Figures 5 and 6. The profiles were measured more or less along the same external streamline as that used for the earlier measurements. Except for the measurements of β the two sets of results are generally very similar, although all the values of H and the various integral thicknesses are greater for the measurements with the slender traverse gear. Figures 7 and 8 compare the streamwise and crossflow profiles at $x = 0$ and near $x = 248$ mm measured with the two traverse gears. In the latter case the difference

is considerable, with the profile nearest to separation being that measured with the least interference. If one can take the liberty of extrapolating the values of θ_{11}, H and β on the basis of the yaw-probe measurements, the values measured with the slender traverse gear are underestimated by about 1/3 of the difference between the results with the original and slender traverse gears; this suggests that at $x = 248$ mm θ_{11} should be increased by 0.06 mm (about 2%), H by 0.057 and β by 3°.

5. Discussion of the measured profiles

In Figure 9 the streamwise profiles measured with the slender traverse gear are compared with the Thompson[7] profiles of equal H and R_θ. The agreement is excellent, providing ample justification for the use of these profiles on swept wings even quite close to the separation line. Figure 10 shows the measured crossflow profiles compared with Mager's[8] representation. When the transverse pressure gradient over the rear has sufficiently dominated the crossflow, Mager's expression appears to be quite satisfactory. At the minimum pressure, and while the crossflow in the initial direction is still not entirely overcome, the representation is unsatisfactory. Because the values of the crossflow thicknesses (δ_2, θ_{12}, θ_{21} and θ_{22}) are generally so small where the Mager representation is least satisfactory, the consequence of inaccuracies in these quantities on calculation methods is probably less serious than Figure 10 would suggest.

In Figure 11 the crossflow velocity is plotted against streamwise velocity and there is a very satisfactory collapse of the data on to sets of straight lines. These results clearly show that Johnston's[9] model, with some modification to allow for the change in direction of the streamline curvature, is capable

of very accurately representing the measured profiles.

Where the measuring stations with the two traverse gears coincide, the profiles measured with the original traverse gear are also shown on Figure 10. The concurrence of the two sets of measurements in the outer part of the boundary layer, near $x = 198$ mm and 248 mm, is significant. The slope of the outer part depends almost entirely on the behaviour of the external flow; the agreement shows that the traverse gear produced a negligible effect on the free stream, so that all the interference was evidently restricted to the boundary layer.

Figure 12 shows the streamwise profiles plotted logarithmically in such a way as to show up regions in which the law of the wall is valid. The values of u_τ ($= \sqrt{\tau_w/\rho}$, where τ_w is the wall shear stress in the streamwise direction) were obtained by plotting the streamwise profiles on a Clauser[10] plot to obtain the skin-friction coefficient. The generally good collapse on to a well established line largely explains the agreement between the measured streamwise profiles and the Thompson profiles.

6. Calculation of the boundary layer development

In Figure 5 the measured values of θ_{11}, H and β are compared with calculations using Cumpsty and Head's[1] method. Three calculations are shown corresponding to slightly different assumptions for the external flow; the reasons for introducing these assumptions are discussed below.

To perform three-dimensional boundary-layer calculations on a swept wing using a system of streamline coordinates the flow outside the boundary layer must be specified in considerable detail; in addition to the pressure gradient along each streamline, it is necessary to know the streamline direction, curvature and

convergence, as well as the distance along the streamline in terms of any other coordinates used. It was necessary to deduce these quantities from the pressure distributions shown in Figure 2 and the dynamic pressure in the working section. In fact, the pressure tappings were too widely spaced along the span and only the downstream set were relevant. The quantities listed above can be found once the components of the velocity outside the boundary layer are known, but the pressure distribution gives only the resultant velocity outside the boundary layer, U_s. To find the spanwise and chordwise components of the external velocity, further independent information is required.

On an infinite swept wing the spanwise velocity, V, is constant over the entire span and chord, and the magnitude of V is immediately obtainable by evaluating the velocity at the leading edge. After making this assumption ($V = V_{le}$, where V_{le} is the velocity on the leading edge) for the present measurements, the calculations represented by the solid lines in Figure 5 were obtained. The agreement is not satisfactory, and in particular the θ_{11} development shows a reduced rate of growth similar to that obtained by Smith[2]. Hand calculations showed that the required growth of θ_{11} could only be obtained, using the measured values of H and β, if the values of θ_{11} used in the calculation were increased well beyond the measured values. This suggested strongly that the gross error was attributable to the data supplied to the boundary layer calculation rather than to the assumptions of the calculations themselves, and consequently a number of more or less arbitrary adjustments were tried.

Attention has been drawn to the assumptions needed for the spanwise velocity. A number of calculations were performed in which the effective value of V over the rear was varied, and the

results of the most successful of these, in which V was assumed to be equal to $1.05V_{le}$, are shown in Figure 5. The agreement in this case is very much better, particularly for θ_{11}, although there is still an appreciable discrepancy between measured and calculated values of H and β. This, however, is possibly attributable to inadequacies in the boundary layer calculation method.

On reflection it is clear that, if V is to be different from the leading-edge value, it should be greater. The tunnel roof and floor constrain the flow so that it is locally parallel to them. Since over most of the chord the U component just outside the boundary layer is larger than in the free-stream, near to the roof and floor the V component must also be larger than in the free stream. It is clearly a gross approximation to assume that the V component is increased by a uniform amount from minimum pressure to the separation line; nevertheless it does demonstrate the sensitivity of the calculations to a fairly plausible increase in spanwise velocity. This sensitivity of the calculations to the precise value of V arises mainly from the increase it produces in the inclination of the external streamlines to the x-direction. This increases the crosswise differentials relative to the streamwise differentials and, whereas it has a small effect directly on the streamwise momentum equation, it has a large effect of the crosswise equation, which in turn has a large effect on the streamwise development. (This behaviour can be deduced from a simple consideration of the magnitude of terms in the respective equations. It was also clearly demonstrated by the successive iterations of the calculation.)

Some calculations were performed in which V was taken as

the leading edge value but the pressure distribution was varied to improve the calculated development. Figure 5 shows the result using the adjusted pressure distribution shown in Figure 2. The level of agreement is similar to that obtained with the measured pressure distribution and $V = 1.05\ V_{le}$. This adjusted pressure distribution would, for example, have required an error of 15 mm in the pressure measured at the separation line (the manometer was alcohol filled and inclined at 30°) and it is most unlikely that consistent errors of this magnitude should have been made.

A further possible explanation has been suggested for the discrepancy between the measurements and the calculation using the measured pressure distribution with $V = V_{le}$. It is that the boundary layers on the tunnel roof and floor led to an additional convergence of the streamlines on the wing. The calculations, however, showed that very large increases in the convergence near to the separation line produced quite small changes in the computed boundary layer development, and this explanation is therefore considered unlikely.

In Figure 13 a final comparison of calculations with measurements is shown; in this case the computed values of H, $R_{\theta 11}$ and β have been used to obtain the streamwise and crosswise velocity profiles. Thompson profiles are used for the streamwise profiles and Mager's representation (together with the Thompson profile) for the crossflow. Figure 10 showed that there are serious inadequacies in the crossflow representation, and to obtain the reasonable overall agreement expected for the initial profile the initial value of β has been doubled. (Although the overall agreement for the initial crossflow is now apparently quite good, there is now, of course, a marked discrepancy close to the surface.) The calculations were performed using the

measured pressure distribution, but taking $V = 1.06V_{le}$, since a 6% increase in V was found to be most satisfactory with this increased initial crossflow. The general level of agreement between the computed and measured profiles is surprisingly good. The discrepancy found at $x = 248$ mm can be explained by the discrepancies in H and β similar to those shown in Figure 5.

7. Conclusions

From the present experiments it is concluded that the development of the boundary layer on a swept wing may be greatly influenced by traverse gear interference, and that the conditions over the rear of an infinite swept wing are very imperfectly simulated by the use of a finite swept wing between boundaries, even where the aspect ratio is reasonably large.

The foregoing conclusions relate to a thick, highly swept section with separation close to the trailing edge, but suggest that, even in less extreme cases, considerable care should be exercised to reduce interference to a minimum and to ensure that conditions are uniform along the span. It is also evident that, unless the aspect ratio is extremely large, it is likely to be unsatisfactory to evaluate the flow outside the boundary layer assuming the spanwise velocity to be constant over the wing; the direction of the flow outside the boundary layer must be accurately measured.

Comparisons of the measurements with calculations by the method of Cumpsty and Head show, as do those of Smith, that the development of streamwise momentum thickness, form parameter and crossflow are considerably underestimated. However, only a small adjustment to the spanwise velocity over the rear of the wing is required to bring the results into quite tolerable agreement.

The necessity for such an adjustment to the spanwise velocity may be plausibly explained by the effect of tunnel constraints.

The streamwise velocity profiles measured are very well described by Thompson's two-dimensional profile family and Mager's representation for the crossflow is generally satisfactory well away from the pressure minimum. The streamwise profiles show, on the whole, a satisfactory collapse on to the law of the wall and the representation for the crossflow proposed by Johnston provides the basis of a very satisfactory description of the crossflow.

References

1. Cumpsty, N.A. and Head, M.R. The calculation of three-dimensional turbulent boundary layers. Part 1: Flow over the rear of an infinite swept wing. Aero. Quart. Vol. XVIII, p.55, 1967.

2. Smith, P.D. Calculation methods for three-dimensional turbulent boundary layers. A.R.C. R & M 3523, 1966.

3. Thompson, B.G.J. Private communication.

4. Head, M.R. Entrainment in the turbulent boundary layer. A.R.C. R & M 3152, 1958.

5. Cumpsty, N.A. and Head, M.R. The calculation of three-dimensional turbulent boundary layers, Part 3: Comparison between calculations and measurement on the leading edge of a swept wing. To be published in the Aero. Quart.

6. Francis, G.P. and Pierce, F.J. An experimental study of skewed turbulent boundary layers in low speed flows. J. Basic Engng., Trans. A.S.M.E., Series D, Vol. 89, p.597, 1967.

7. Thompson, B.G.J. A new two-parameter family of mean velocity profiles for incompressible turbulent boundary layers on smooth walls. A.R.C. R & M 3463, 1965.

8. Mager, A. Generalisation of the boundary layer momentum integral equations to three-dimensional flows, including those of rotating systems. NACA Report 1067, 1952.

9. Johnston, J.P. On the three-dimensional turbulent boundary layer generated by secondary flow.
J. Basic Engng., Trans. A.S.M.E., Series D, Vol. 82, p.233, 1960.

10. Clauser, F.H. Turbulent boundary layers in adverse pressure gradients.
J. Aero. Sci. Vol. 21, p.91, 1954.

Table I

Coordinates of wing surface

Xmm	0	1.28	2.53	3.83	5.26	6.55	7.86	9.19	10.50	11.42	12.70	13.93
Zmm	0	5.45	7.33	8.81	9.81	10.23	10.80	11.17	11.35	11.42	11.40	11.30

Xmm	15.22	16.50	17.78	19.07	21.6	24.15	26.7	29.2	31.8	34.3	36.8
Zmm	11.18	10.95	10.68	10.38	9.70	8.95	7.94	7.05	6.14	5.06	4.00

Xmm	39.4	42.0	44.5	45.8
Zmm	2.86	1.74	0.61	0

Table 2

Measured Boundary Layer Profiles

Using Slender Traverse Gear

ζ 10^{-3} in	u/U_s	v/U_s	ζ 10^{-3} in	u/U_s	v/U_s
x = 0 162.0	1.000	0.000	x = 0.650 ft		
137.0	0.999	- 0.003	669.0	1.000	0.000
112.0	0.993	- 0.012	569.0	0.996	0.000
87.0	0.968	- 0.027	469.0	0.975	0.005
62.0	0.913	- 0.044	419.0	0.945	0.018
52.0	0.877	- 0.050	369.0	0.896	0.032
37.0	0.820	- 0.055	319.0	0.850	0.052
22.0	0.738	- 0.052	269.0	0.793	0.076
17.0	0.702	- 0.052	219.0	0.739	0.097
12.0	0.671	- 0.049	169.0	0.681	0.122
10.0	0.653	- 0.045	119.0	0.619	0.143
8.0	0.628	- 0.034	94.0	0.586	0.152
6.0	0.603	- 0.032	69.0	0.549	0.158
4.0	0.553	- 0.028	44.0	0.507	0.162
2.0	0.484	- 0.025	29.0	0.473	0.162
0.0	0.000	0.000	19.0	0.443	0.158
			9.0	0.386	0.151
x = 0.217 ft			4.0	0.332	0.127
224.0	1.000	0.000	0.0	0.000	0.000
194.0	0.993	0.000			
169.0	0.974	- 0.006	x = 0.813 ft		
144.0	0.937	- 0.011	889.0	1.000	0.000
119.0	0.888	- 0.007	789.0	0.991	0.002
94.0	0.823	0.002	689.0	0.947	0.019
69.0	0.754	0.013	589.0	0.882	0.052
44.0	0.674	0.030	489.0	0.804	0.095
29.0	0.619	0.040	389.0	0.719	0.141
19.0	0.574	0.054	289.0	0.632	0.187
14.0	0.548	0.053	242.0	0.603	0.186
9.0	0.511	0.057	192.0	0.560	0.206
4.0	0.439	0.053	189.0	0.549	0.219
2.0	0.376	0.045	139.0	0.507	0.232
0.0	0.000	0.000	92.0	0.469	0.227
			89.0	0.460	0.236
x = 0.446 ft			64.0	0.427	0.241
395.0	1.000	0.000	42.0	0.413	0.221
345.0	0.996	0.000	39.0	0.395	0.226
295.0	0.967	0.003	17.0	0.363	0.208
245.0	0.908	0.015	7.0	0.327	0.197
195.0	0.839	0.030	4.0	0.308	0.193
145.0	0.761	0.054	0.0	0.000	0.000
120.0	0.719	0.066			
95.0	0.676	0.078			
70.0	0.634	0.083			
45.0	0.577	0.101			
20.0	0.502	0.106			
10.0	0.436	0.104			
5.0	0.364	0.102			
2.0	0.280	0.080			
0.0	0.000	0.000			

Table 2 (contd)

Using Original Traverse Gear

ζ 10^{-3} in	u/U_s	v/U_s	ζ 10^{-3} in	u/U_s	v/U_s
x = 0 157.0	1.000	0.000	x = 0.491 ft		
132.0	0.999	0.003	391.0	1.000	0.000
117.0	0.995	- 0.006	341.0	0.994	0.000
107.0	0.989	- 0.012	316.0	0.985	0.004
87.0	0.963	- 0.021	291.0	0.965	0.005
67.0	0.930	- 0.021	266.0	0.942	0.010
57.0	0.903	- 0.042	241.0	0.914	0.015
47.0	0.872	- 0.050	216.0	0.882	0.024
37.0	0.832	- 0.055	191.0	0.851	0.030
27.0	0.786	- 0.052	166.0	0.815	0.039
22.0	0.759	- 0.051	141.0	0.776	0.050
17.0	0.726	- 0.051	121.0	0.746	0.058
12.0	0.684	- 0.050	91.0	0.700	0.072
7.0	0.615	- 0.040	66.0	0.658	0.079
5.0	0.587	- 0.036	41.0	0.610	0.084
3.0	0.497	- 0.027	21.0	0.553	0.083
0.0	0.000	0.000	11.0	0.493	0.076
			6.0	0.419	0.066
x = 0.175 ft			4.0	0.361	0.059
227.0	1.000	0.000	3.0	0.312	0.050
177.0	0.995	- 0.003	2.0	0.261	0.045
152.0	0.978	- 0.006	0.0	0.000	0.000
127.0	0.944	- 0.015			
102.0	0.895	- 0.018	x = 0.645 ft		
77.0	0.833	- 0.014	602.0	1.000	0.000
52.0	0.763	- 0.003	502.0	0.997	0.006
37.0	0.719	0.003	452.0	0.983	0.009
27.0	0.672	0.007	402.0	0.952	0.021
17.0	0.620	0.015	352.0	0.908	0.034
7.0	0.522	0.021	302.0	0.860	0.048
4.0	0.452	0.023	252.0	0.810	0.070
2.0	0.363	0.028	202.0	0.755	0.094
0.0	0.000	0.000	152.0	0.697	0.119
			102.0	0.639	0.138
x = 0.333 ft			52.0	0.570	0.148
301.0	1.000	0.000	27.0	0.521	0.145
276.0	0.997	0.000	17.0	0.485	0.140
251.0	0.990	0.000	7.0	0.408	0.122
226.0	0.974	0.000	3.0	0.333	0.105
201.0	0.948	0.000	2.0	0.306	0.099
176.0	0.911	0.002	0.0	0.000	0.000
151.0	0.870	0.006			
126.0	0.825	0.016			
101.0	0.782	0.030			
76.0	0.731	0.042			
51.0	0.675	0.056			
26.0	0.607	0.064			
11.0	0.532	0.065			
6.0	0.481	0.064			
4.0	0.429	0.057			
3.0	0.400	0.055			
0.0	0.000	0.000			

Table 2 (contd)

Using Original Traverse Gear (contd)

ζ 10^{-3} in	u/U_s	v v/U_s	ζ 10^{-3} in	u/U_s	v/U_s
x = 0.817 ft			x = 0.875 ft		
873.0	1.000	0.000	945.0	1.000	0.000
823.0	0.998	0.000	895.0	0.999	0.001
723.0	0.994	0.004	845.0	0.994	0.003
623.0	0.959	0.020	745.0	0.965	0.012
523.0	0.892	0.049	645.0	0.905	0.038
423.0	0.810	0.090	545.0	0.829	0.077
323.0	0.727	0.127	445.0	0.756	0.117
223.0	0.641	0.172	395.0	0.718	0.139
173.0	0.604	0.187	345.0	0.679	0.158
123.0	0.562	0.201	295.0	0.643	0.176
73.0	0.512	0.204	245.0	0.601	0.196
48.0	0.480	0.198	195.0	0.565	0.208
23.0	0.429	0.181	145.0	0.525	0.220
8.0	0.330	0.137	95.0	0.484	0.220
4.0	0.229	0.092	45.0	0.430	0.211
2.0	0.171	0.062	25.0	0.393	0.197
0.0	0.000	0.000	5.0	0.260	0.134
			3.0	0.218	0.115
			2.0	0.176	0.096
			0.0	0.000	0.000

Table 3

Boundary Layer Integral Thicknesses

x ft	δ_1^* 10^{-3}ft	θ_{11} 10^{-3}ft	δ_2^* 10^{-3}ft	θ_{12} 10^{-3}ft	θ_{21} 10^{-3}ft	θ_{22} 10^{-3}ft
Slender Traverse Gear						
0.000	1.42	0.999	+ 0.384	- 0.060	+ 0.324	- 0.016
0.217	3.25	2.16	- 0.195	+ 0.098	- 0.097	- 0.012
0.466	6.37	4.12	- 1.34	+ 0.464	- 0.879	- 0.101
0.650	10.34	6.58	- 3.53	+ 1.238	- 2.29	- 0.425
0.813	18.94	11.11	- 8.51	+ 3.39	- 5.13	- 1.526
Original Traverse Gear						
0.000	1.38	0.952	+ 0.357	- 0.056	+ 0.301	- 0.014
0.175	2.57	1.76	+ 0.088	+ 0.006	+0.095	- 0.002
0.333	4.17	2.84	- 0.521	+ 0.171	- 0.350	- 0.025
0.491	5.78	3.90	- 1.166	+ 0.348	- 0.817	- 0.072
0.645	8.93	5.91	- 3.18	+ 0.982	- 2.19	- 0.342
0.813	15.34	9.51	- 6.64	+ 2.34	- 4.30	- 1.014
0.875	19.27	11.49	- 8.43	+ 3.23	- 5.20	- 1.426

Table 4

Pressure Distribution at Downstream Set of Pressure Tapping

	$X/_c$	x feet	$\frac{p-p_s}{\frac{1}{2}U_{1\infty}^2}$	
l.e.	0.000		1.000	
	0.002		1.000	
	0.004		0.903	
	0.015		0.548	
	0.033		- 0.028	
	0.058		- 0.712	
	0.089		- 1.52	
	0.125		- 2.08	$\frac{1}{2}\rho U_\infty^2$ = 12.1 cm alcohol
	0.164		- 2.55	
	0.207		- 2.75	
	-	0.000	-	$\frac{1}{2}U_{1\infty}^2$ = 2.82 cm alcohol
	0.250	0.370	- 2.64	
	0.305	0.121	- 2.26	
	0.36	0.204	- 1.76	U_∞ = 133 ft/sec
	0.415	0.291	- 1.49	
	0.468	0.371	- 1.26	
	0.523	0.456	- 1.08	$\frac{U_\infty}{\nu}$ = 0.918. 10^6 ft^{-1}
	0.574	0.539	- 0.888	
	0.626	0.622	- 0.728	
	0.678	0.708	- 0.612	
	0.729	0.790	- 0.532	
	0.781	0.875	- 0.480	
	0.833	0.958	- 0.426	
	0.884	1.041	- 0.408	
	0.937	1.126	- 0.408	
	0.989	1.216	- 0.426	
	1.000	1.30	-	

Table 5

Data used for calulculations

a) using measured pressure distribution

b) assuming $V = V_{1e}$

x	S	$U_s/U_{1\infty}$	$\frac{1}{U_s}\frac{\partial U_s}{\partial s}$	$\frac{1}{h_2}\frac{\partial h_2}{\partial s}$	tan α
0.000	0.000	2.640	- 0.0833	- 0.0734	0.937
0.037	0.053	2.627	- 0.200	- 0.179	0.948
0.121	0.166	2.547	- 0.2873	- 0.2896	1.003
0.204	0.285	2.457	- 0.2547	- 0.2987	1.082
0.291	0.416	2.393	- 0.1928	- 0.2542	1.148
0.371	0.540	2.337	- 0.1554	- 0.2296	1.215
0.456	0.675	2.298	- 0.1250	- 0.2012	1.268
0.538	0.810	2.259	- 0.1024	- 0.1808	1.328
0.622	0.951	2.234	- 0.0823	- 0.1548	1.370
0.708	1.099	2.205	- 0.0666	- 0.1350	1.423
0.790	1.242	2.191	- 0.0522	- 0.1102	1.453
0.875	1.394	2.172	- 0.0366	- 0.0816	1.493
0.958	1.543	2.166	- 0.0218	- 0.0496	1.505
1.041	1.694	2.158	- 0.0069	- 0.0162	1.525
1.126	1.849	2.162	0.0084	0.0193	1.516
1.216	2.012	2.163	0.0238	0.0546	1.512

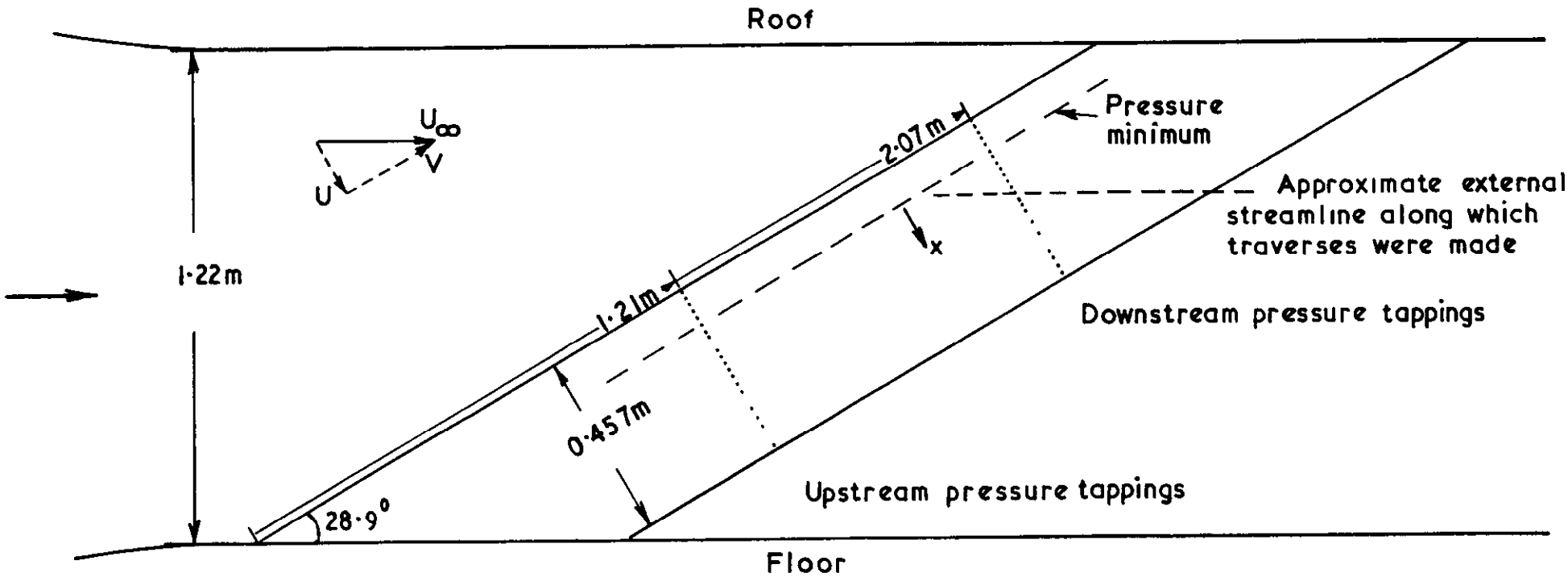

FIG. 1 Schematic view of the wing in the tunnel

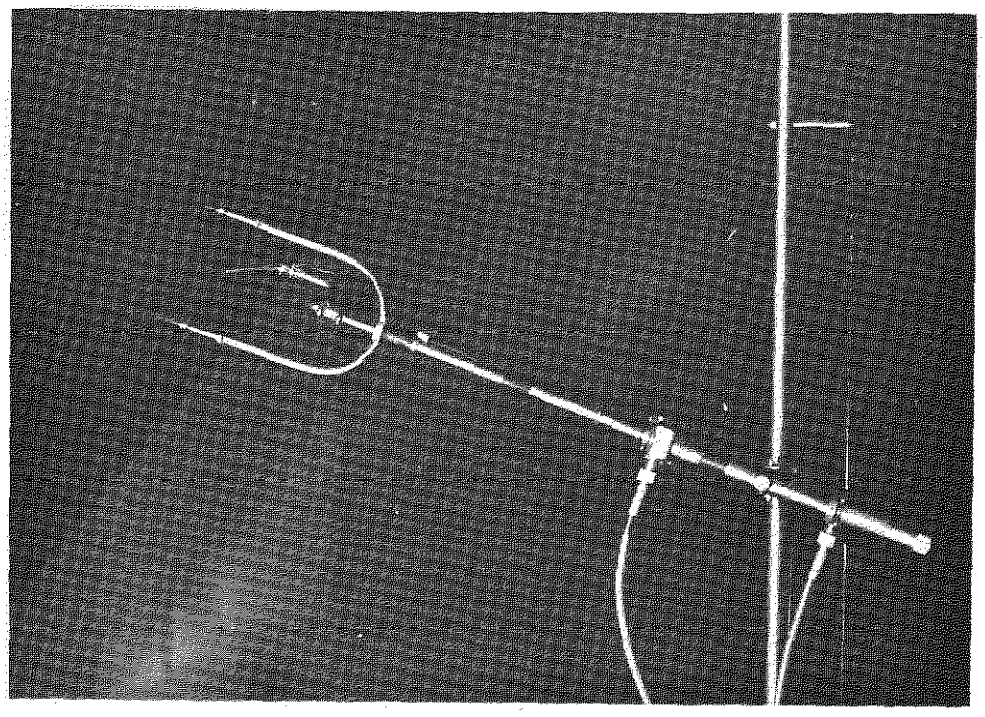

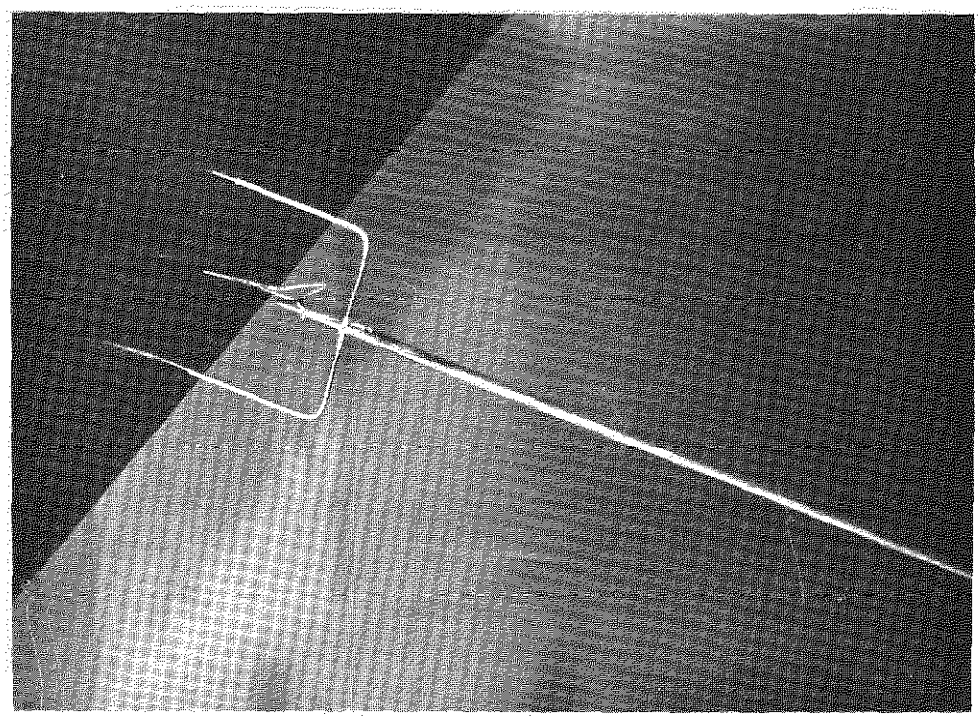

FIG. 2 Photographs, to equal scale, of the original and slender traverse gears

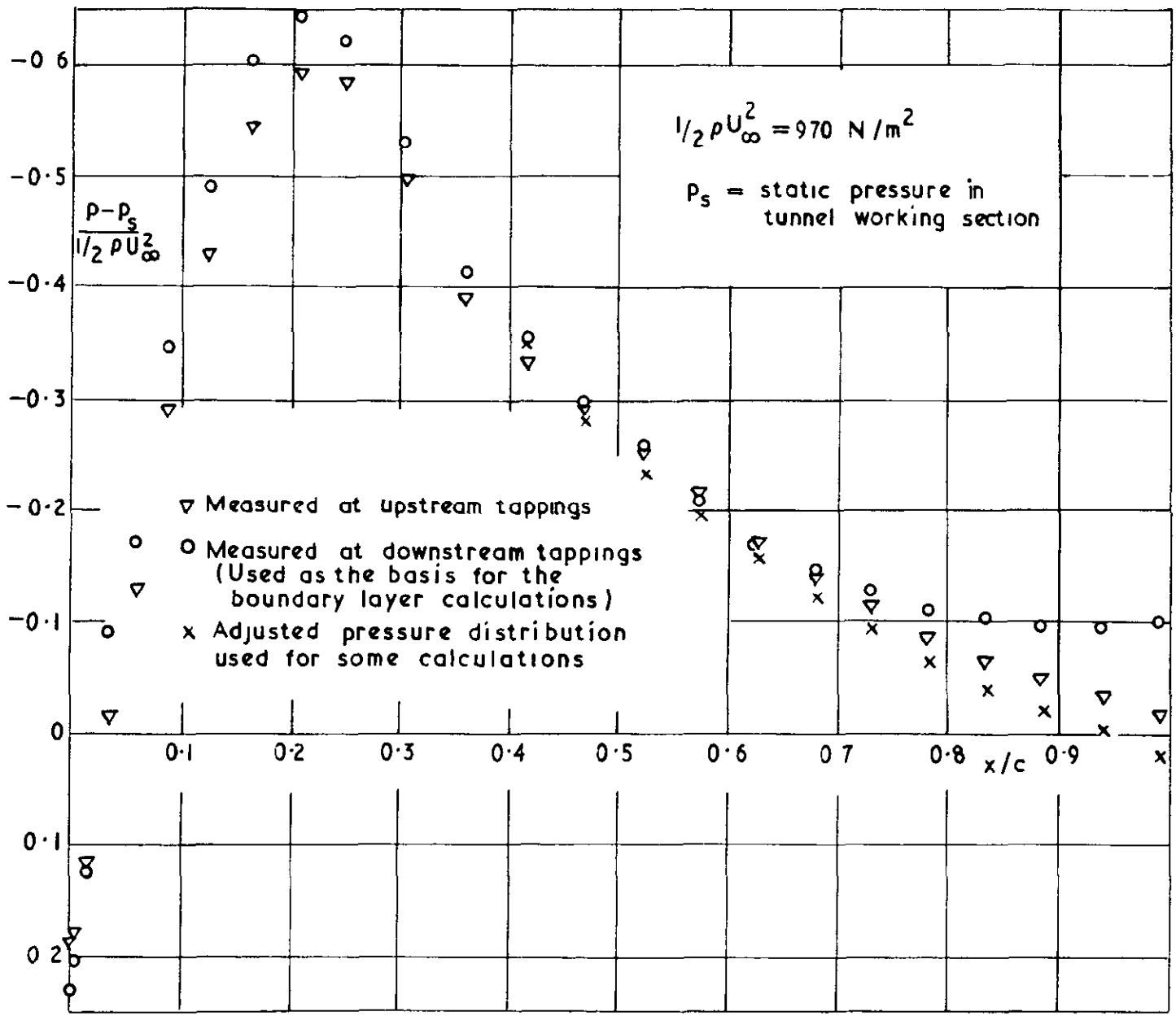

FIG. 3 Static pressure distribution over the wing surface

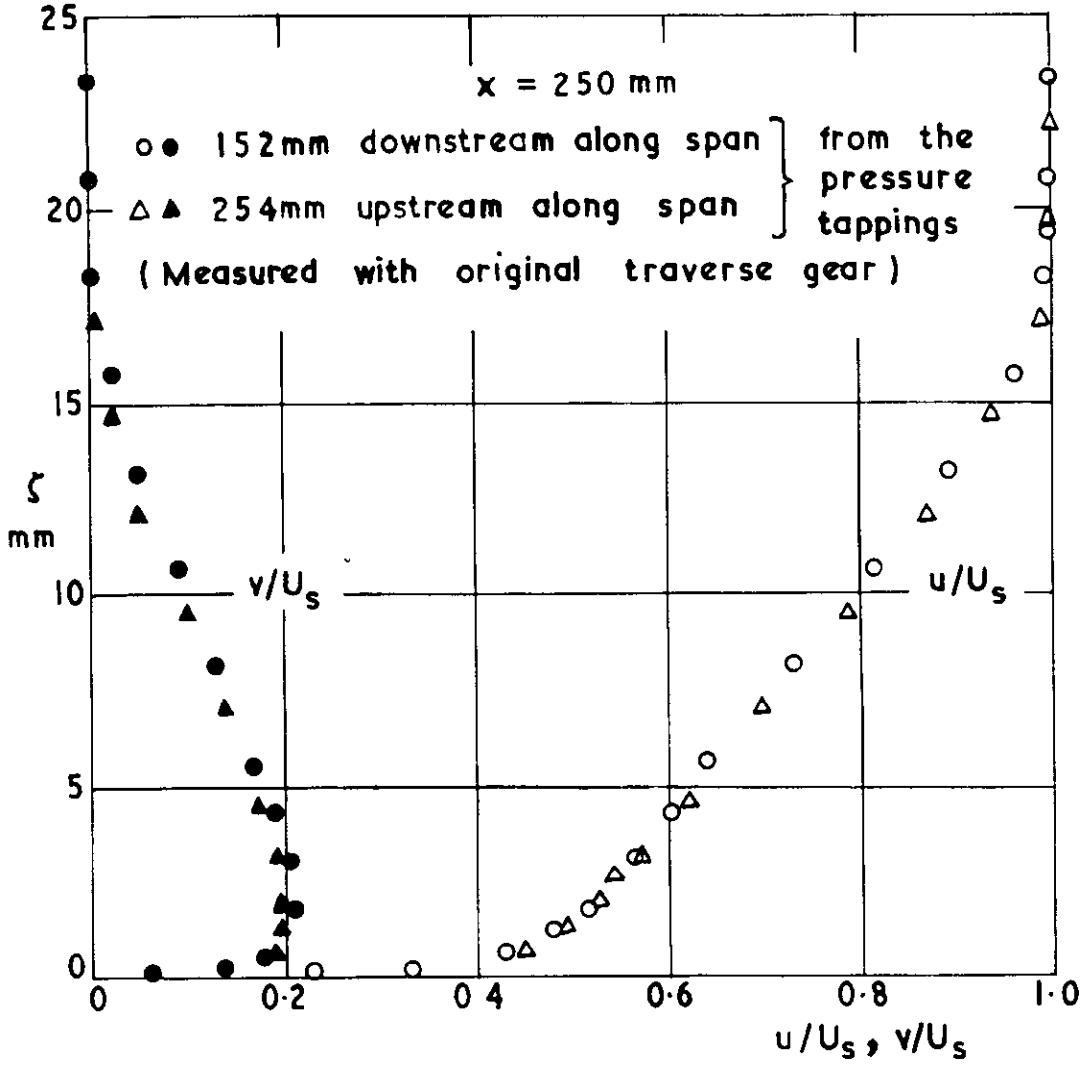

FIG 4 Streamwise and crossflow profiles measured at the same chordwise positions but at different spanwise positions

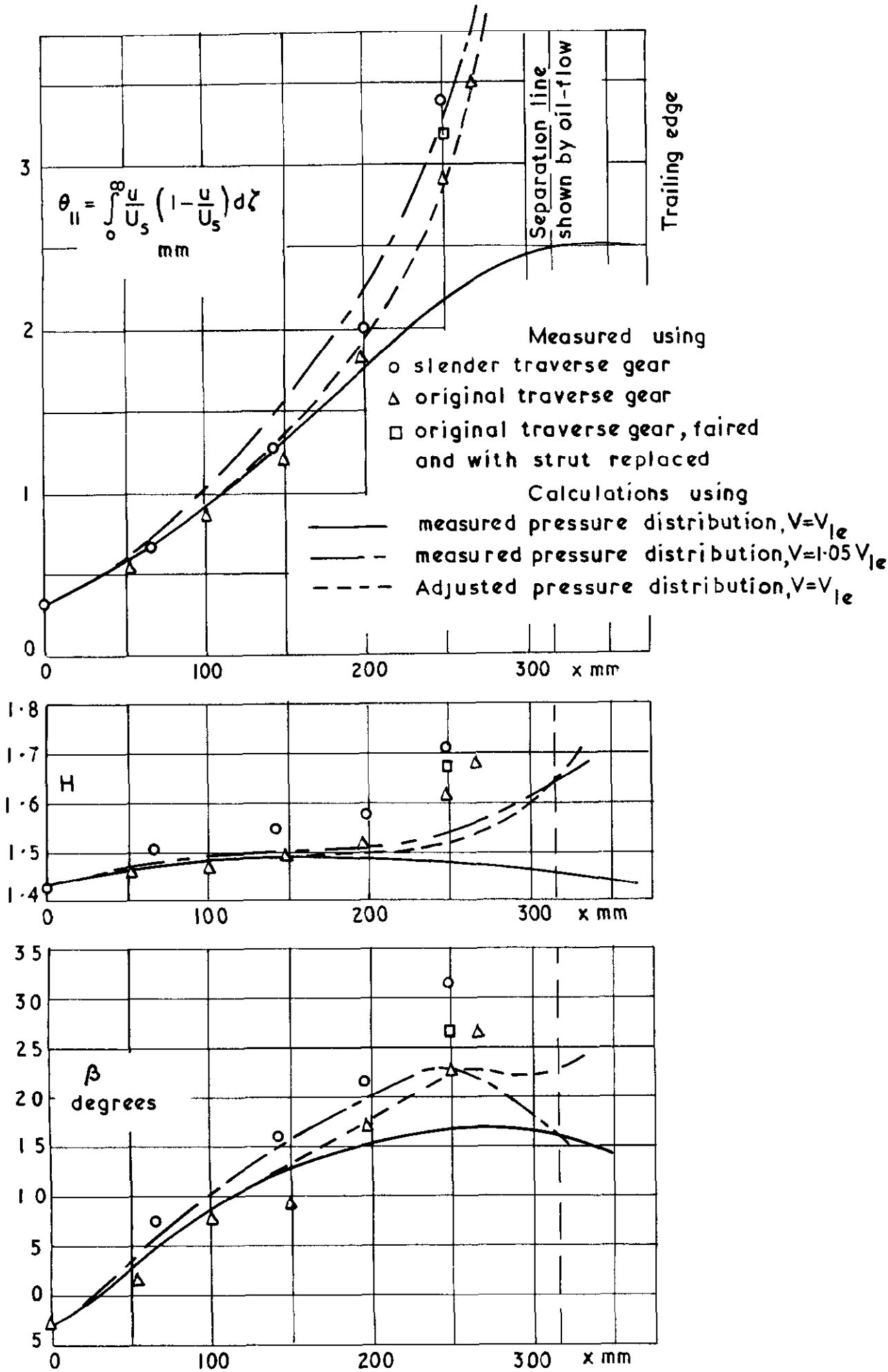

FIG.5 Comparison of measured and calculated boundary layer development

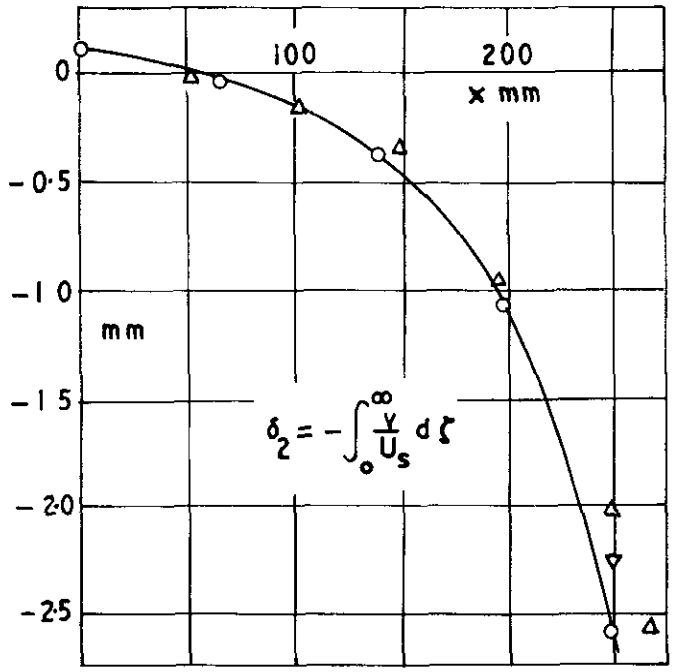

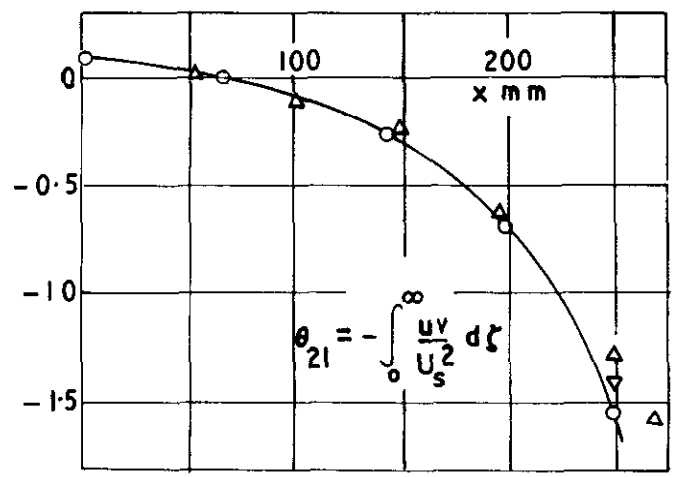

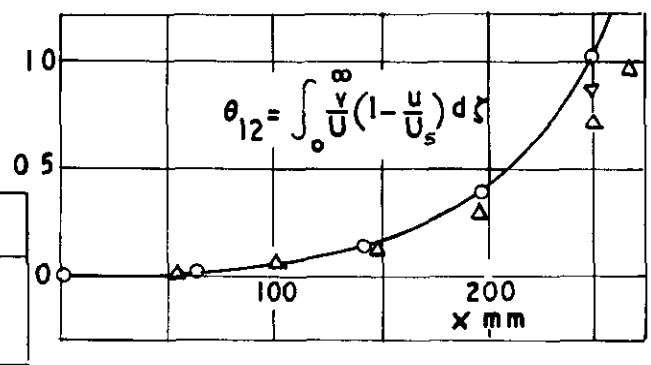

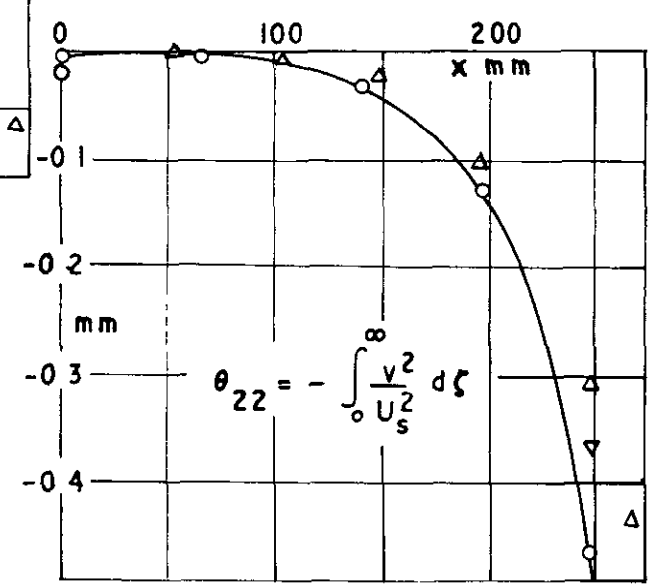

o Measured with slender traverse gear
Δ Measured with original traverse gear
∇ Measured with original traverse gear, faired and with strut replaced

FIG 6 Measured crossflow integral thicknesses

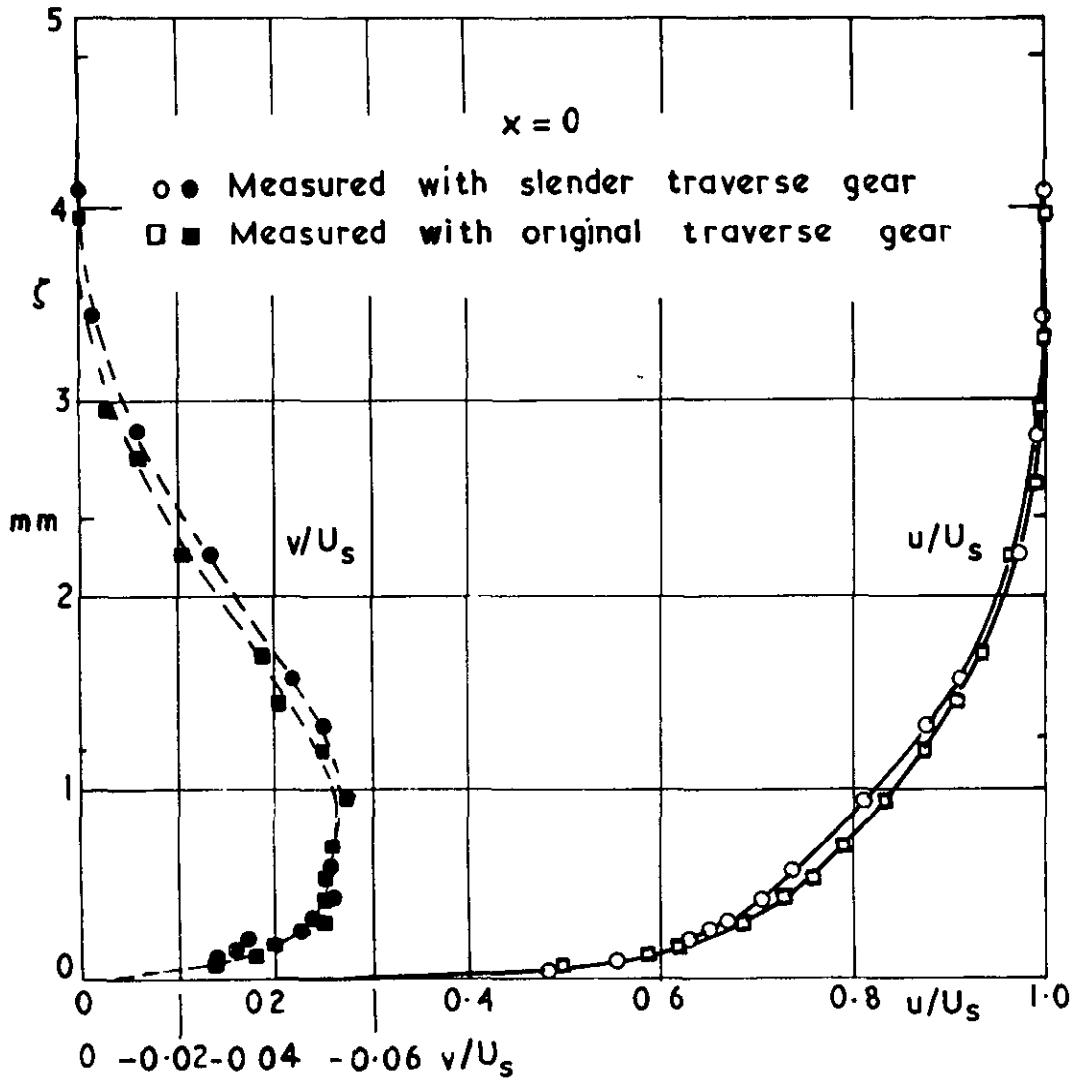

FIG.7 Comparison of velocity profiles measured with two traverse gears at the start of the adverse pressure gradient

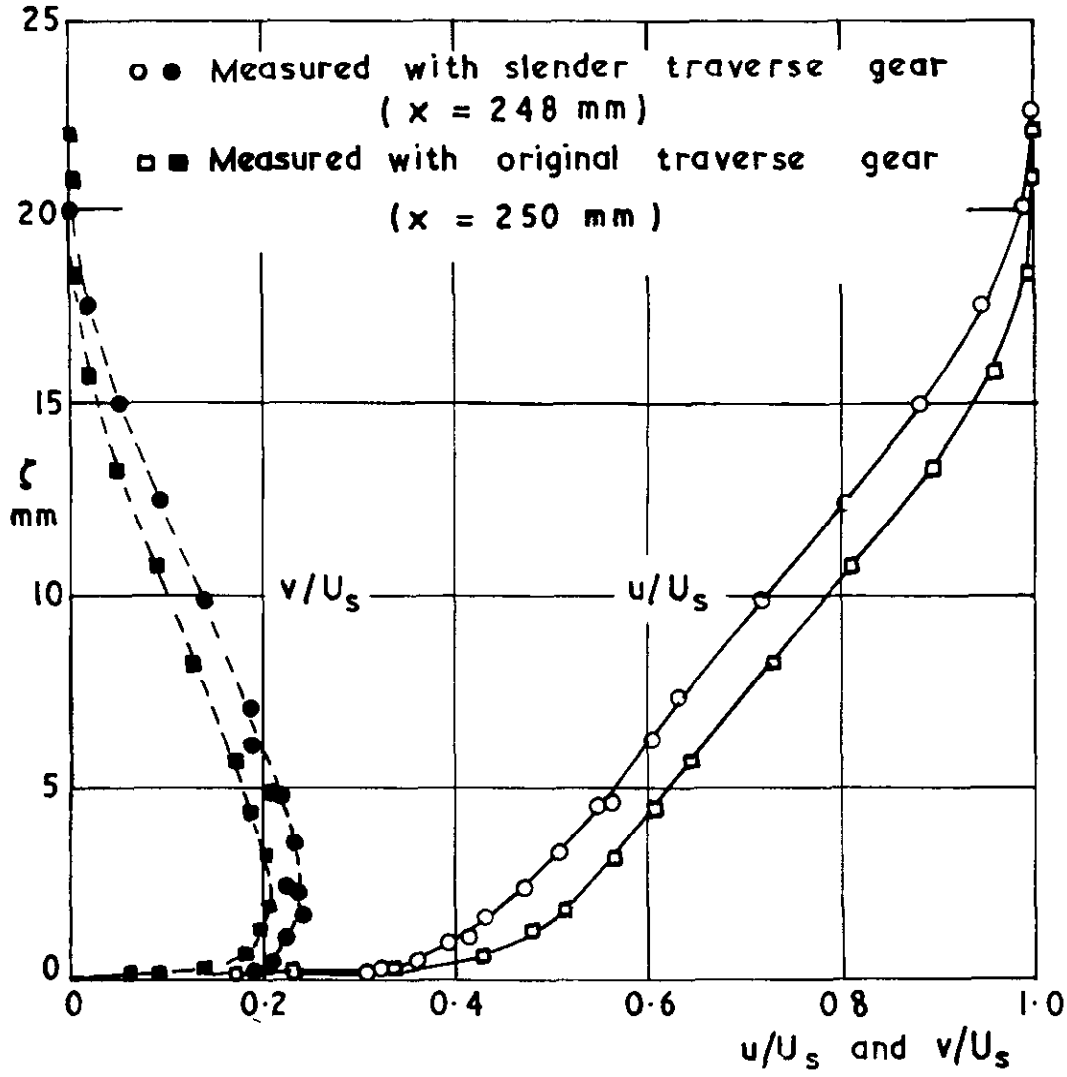

FIG 8 Comparison of velocity profiles measured with two traverse gears near x = 248 mm

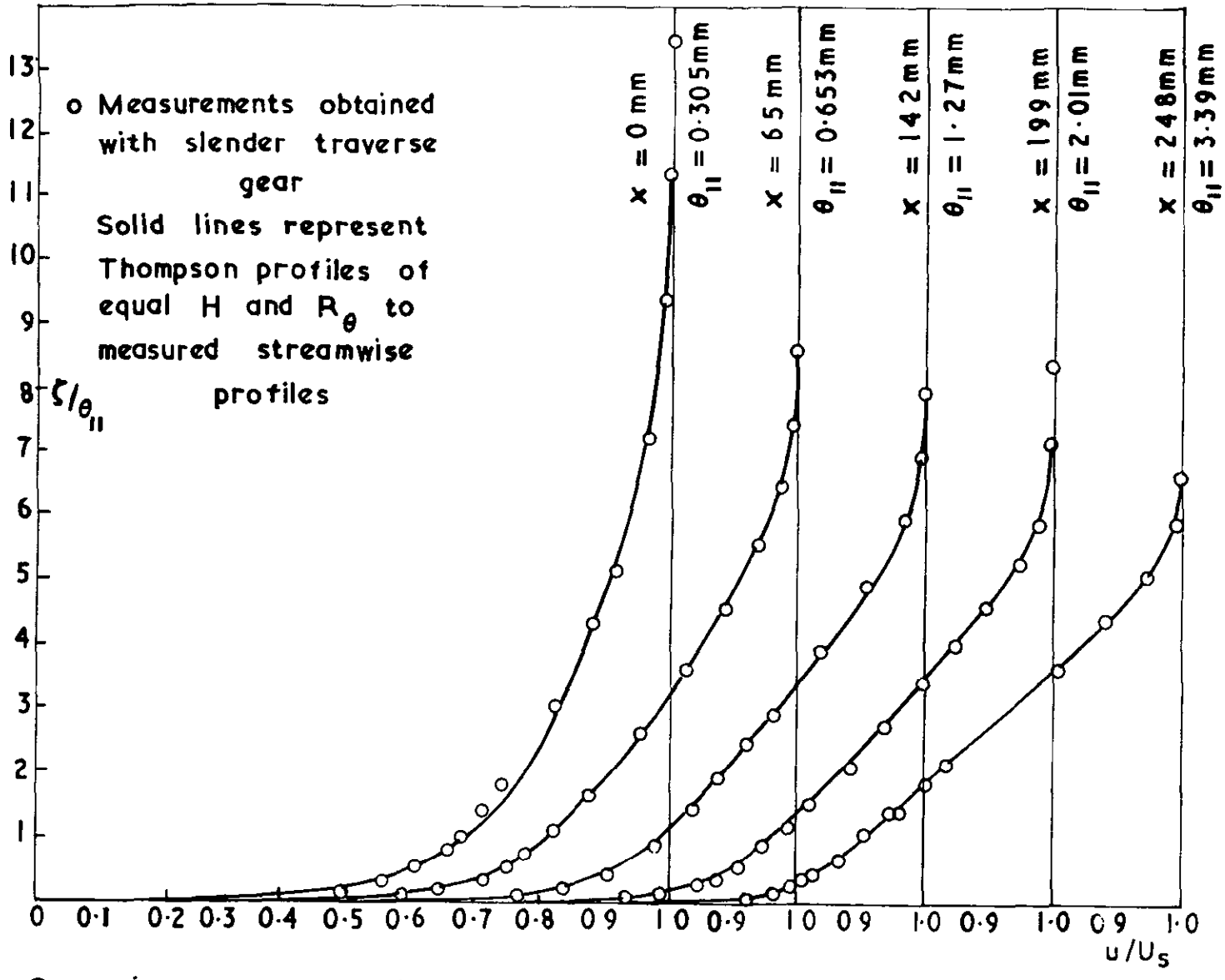

FIG 9 Comparison of measured streamwise velocity profiles with the corresponding profiles from the Thompson profile family

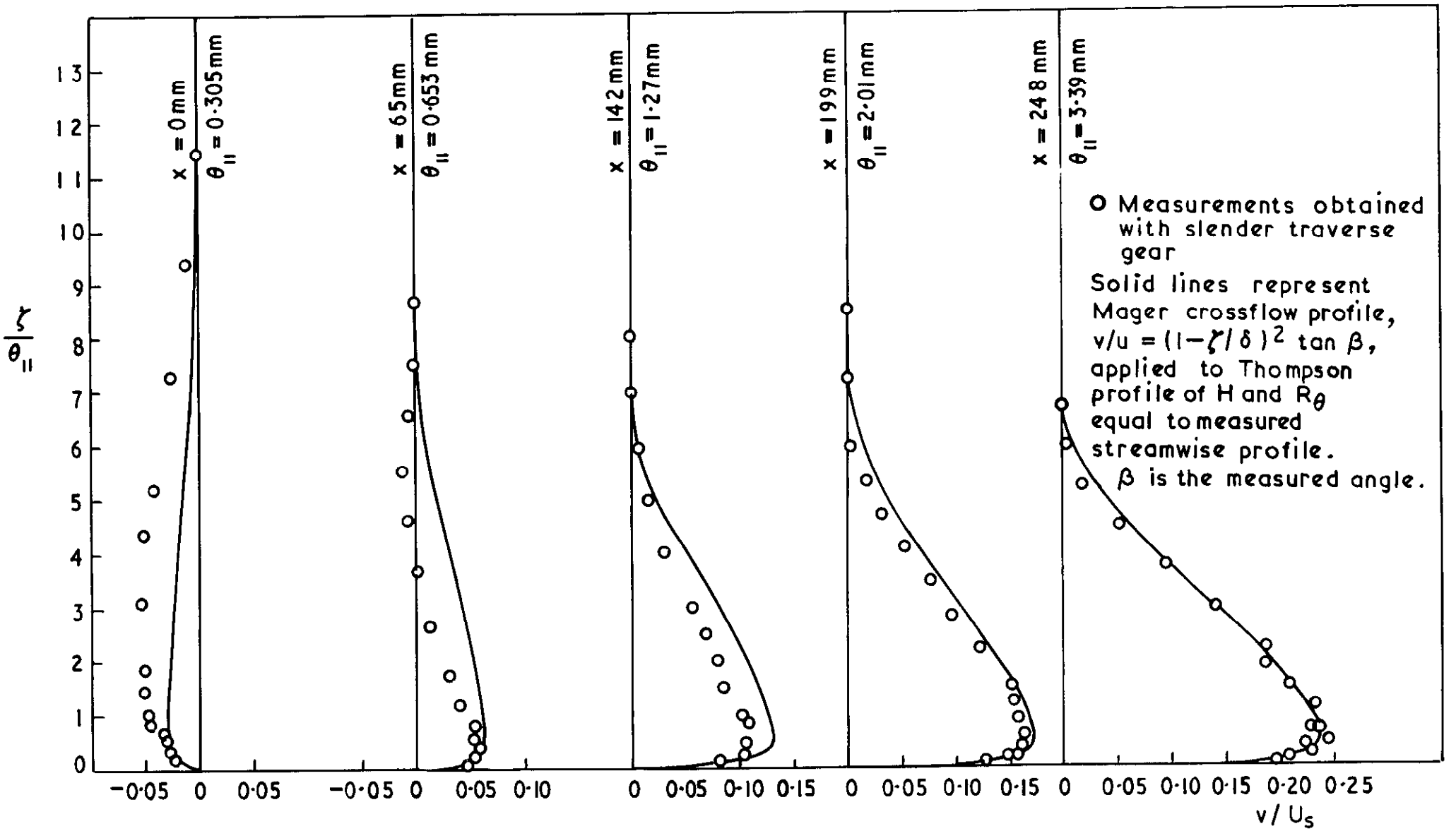

FIG. 10 Comparison of measured crossflow profiles with profiles from the Mager representation applied to Thompson profiles.

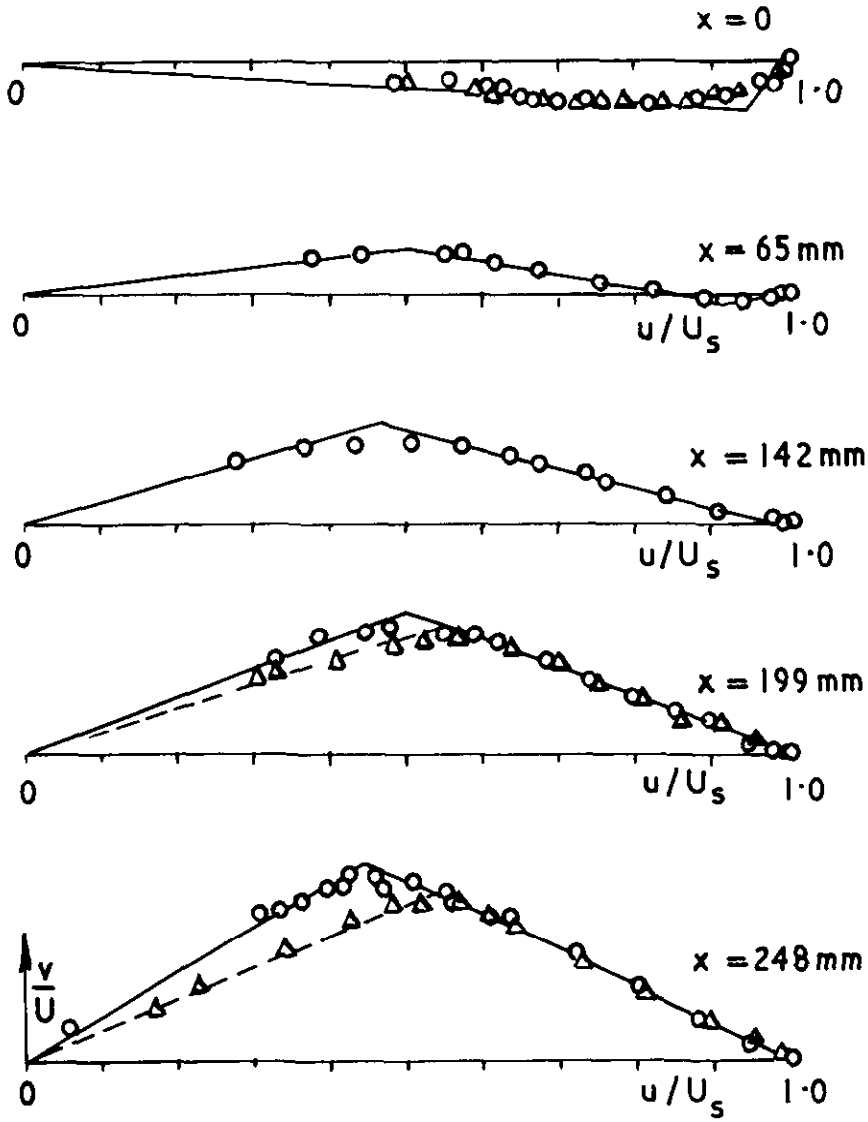

The streamwise and crossflow velocities are shown here to the same scale

o Measurements using slender traverse gear

Δ Measurements using original traverse gear

FIG. 11 Triangular plots of measured velocity profiles

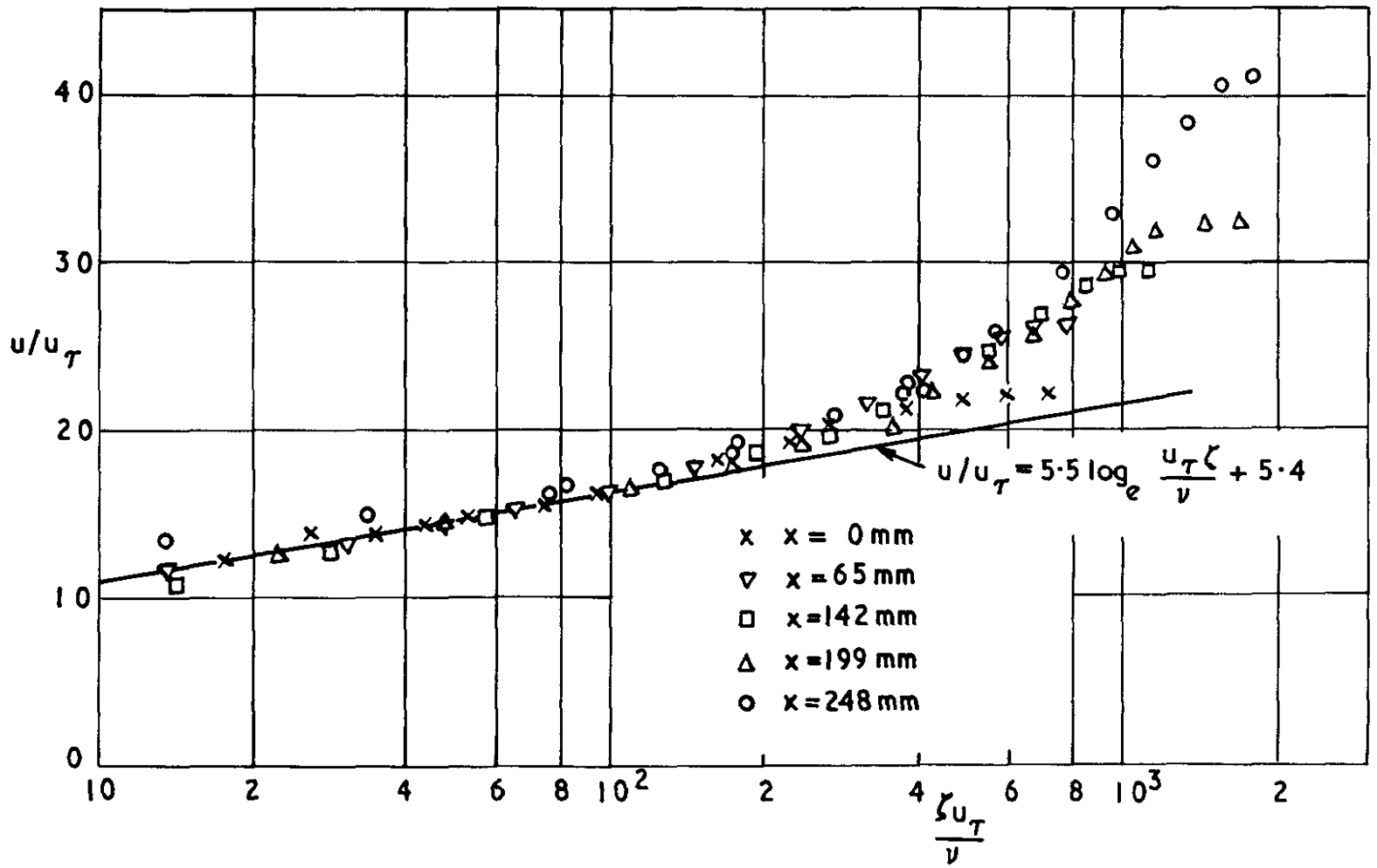

FIG. 12 Streamwise velocity profiles measured with the slender traverse gear

o Streamwise
Δ Crossflow
} velocities measured with slender traverse gear

Solid lines show Thompson profiles and Mager crossflow profiles for values of $H, R_{\theta_{11}}$ and β obtained from the calculations

The initial value of the crossbow angle, β, was doubled for this calculation to improve the overall agreement between the initial measured crossflow profile and the Mager representation.

The calculations were performed using the measured pressure distribution and assuming $V = 1{\cdot}06\, V_{le}$

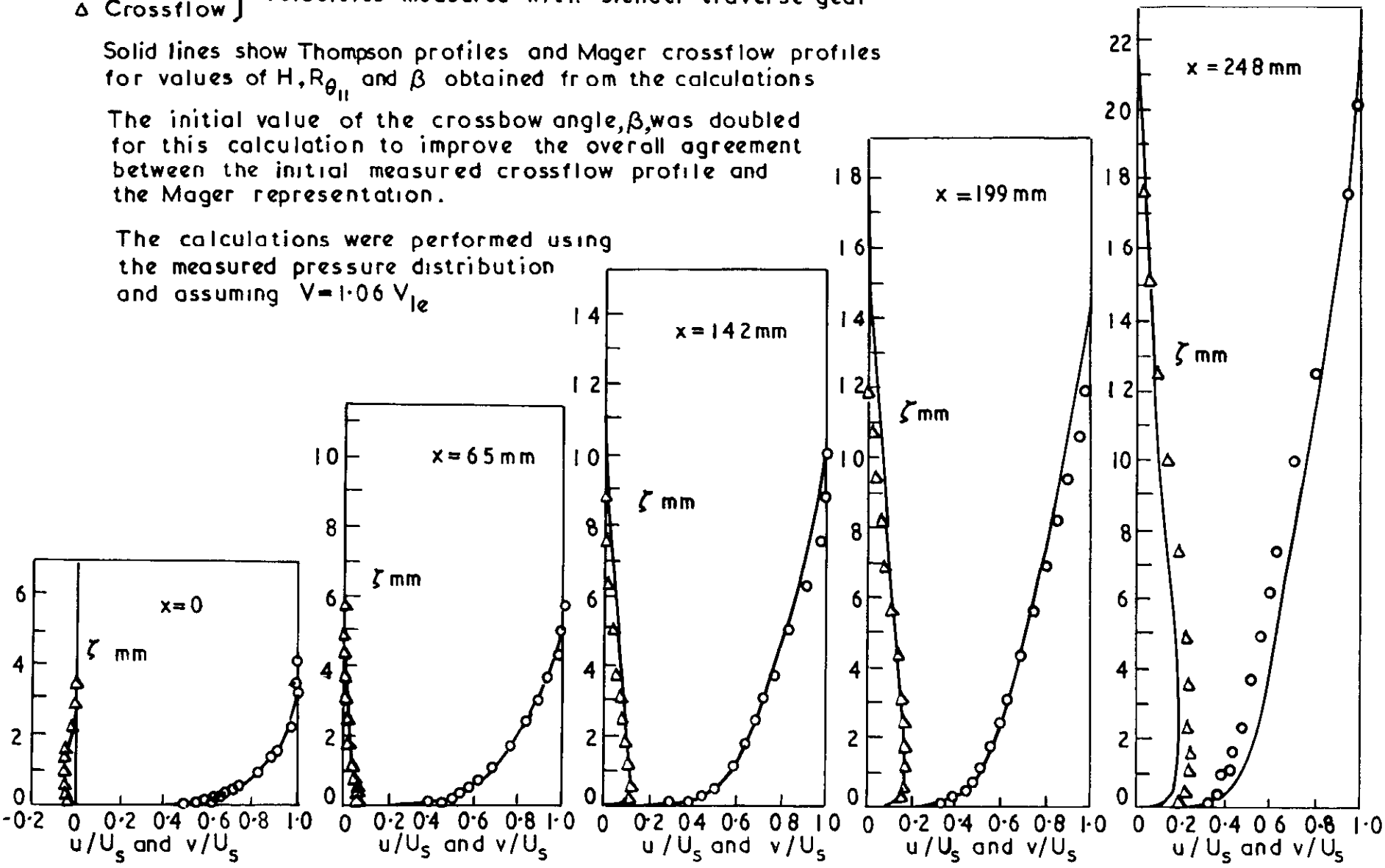

FIG.13 Comparison of measured and calculated velocity profiles

A.R.C. C.P.No.1077
March, 1969
Cumpsty, N. A. and Head, M. R.

THE CALCULATION OF THREE-DIMENSIONAL TURBULENT BOUNDARY LAYERS
PART IV: COMPARISON OF MEASUREMENTS WITH CALCULATIONS ON THE REAR OF A SWEPT WING

A boundary-layer development was measured on the rear of a wing swept at 61°. The measurements approximately followed an external streamline from the neighbourhood of the separation line. Unfortunately the flow was found to be surprisingly sensitive to traverse gear interference. Moreover, the constraint imposed by the wind tunnel walls was sufficient to throw grave doubts on the use of the assumption of constant spanwise velocity/

A.R.C. C.P.No.1077
March, 1969
Cumpsty, N. A. and Head, M. R.

THE CALCULATION OF THREE-DIMENSIONAL TURBULENT BOUNDARY LAYERS
PART IV: COMPARISON OF MEASUREMENTS WITH CALCULATIONS ON THE REAR OF A SWEPT WING

A boundary-layer development was measured on the rear of a wing swept at 61°. The measurements approximately followed an external streamline from the neighbourhood of the separation line. Unfortunately the flow was found to be surprisingly sensitive to traverse gear interference. Moreover, the constraint imposed by the wind tunnel walls was sufficient to throw grave doubts on the use of the assumption of constant spanwise velocity/

A.R.C. C.P.No.1077
March, 1969
Cumpsty, N. A. and Head, M. R.

THE CALCULATION OF THREE-DIMENSIONAL TURBULENT BOUNDARY LAYERS
PART IV: COMPARISON OF MEASUREMENTS WITH CALCULATIONS ON THE REAR OF A SWEPT WING

A boundary-layer development was measured on the rear of a wing swept at 61°. The measurements approximately followed an external streamline from the neighbourhood of the separation line. Unfortunately the flow was found to be surprisingly sensitive to traverse gear interference. Moreover, the constraint imposed by the wind tunnel walls was sufficient to throw grave doubts on the use of the assumption of constant spanwise velocity/

velocity to compute the external flow behaviour from the measured pressure distribution.

Comparison of the measurements with calculations using the method proposed by Cumpsty and Head showed the growth of streamwise momentum thickness, form parameter and crossflow to be seriously underestimated. However, only a small adjustment to the spanwise velocity outside the boundary layer over the rear of the wing was sufficient to bring the results into tolerable agreement. The necessity for such an adjustment to the spanwise velocity may be plausibly explained by the effect of tunnel constraints.

velocity to compute the external flow behaviour from the measured pressure distribution.

Comparison of the measurements with calculations using the method proposed by Cumpsty and Head showed the growth of streamwise momentum thickness, form parameter and crossflow to be seriously underestimated. However, only a small adjustment to the spanwise velocity outside the boundary layer over the rear of the wing was sufficient to bring the results into tolerable agreement. The necessity for such an adjustment to the spanwise velocity may be plausibly explained by the effect of tunnel constraints.

velocity to compute the external flow behaviour from the measured pressure distribution.

Comparison of the measurements with calculations using the method proposed by Cumpsty and Head showed the growth of streamwise momentum thickness, form parameter and crossflow to be seriously underestimated. However, only a small adjustment to the spanwise velocity outside the boundary layer over the rear of the wing was sufficient to bring the results into tolerable agreement. The necessity for such an adjustment to the spanwise velocity may be plausibly explained by the effect of tunnel constraints.

D119297/1/146915 K3 11/69 P

Printed and published by
HER MAJESTY'S STATIONERY OFFICE

To be purchased from
49 High Holborn, London WC1
13a Castle Street, Edinburgh EH2 3AR
109 St Mary Street, Cardiff CF1 1JW
Brazennose Street, Manchester M60 8AS
50 Fairfax Street, Bristol BS1 3DE
258 Broad Street, Birmingham 1
7 Linenhall Street, Belfast BT2 8AY
or through any bookseller

Printed in England

C.P. No. 1077

SBN 11 470277 2